Available online at www.sciencedirect.com
SCIENCE DIRECT®
Journal of Solid State Chemistry 178 (2005) 928–936
JOURNAL OF SOLID STATE CHEMISTRY
www.elsevier.com/locate/jssc

Morphological and magnetic study of $CaMnO_{3-x}$ oxides obtained from different routes

Izaskun Gil de Muro, Maite Insausti, Luis Lezama, Teófilo Rojo*

Departamento de Química Inorgánica, Facultad de Ciencias, Universidad del País Vasco, Apdo 644, ES 48080 Bilbao, Spain

Received 11 May 2004; received in revised form 25 June 2004; accepted 25 June 2004

Abstract

The $CaMnO_{3-x}$ ($x = 0$ and 0.02) mixed oxide was synthesized from both thermal treatment of the $[CaMn(C_3H_2O_4)_2(H_2O)_4]$ metallo-organic precursor and ceramic method. In the case of the latter method, temperatures of 1350 °C and 50 h were necessary; however, lower temperatures, 800 °C, and shorter reaction times, 15 h, were utilized in the attainment of the mixed oxide from the precursor. As a consequence, the morphology of the different products is clearly different. The samples exhibit three-dimensional antiferromagnetic ordering with T_N near 120 K, and a low-dimensional antiferromagnetic ordering at high temperatures. The presence of a ferromagnetic component above T_N was also observed in both compounds, it is slightly stronger in the phase prepared by the ceramic route.

Keywords: Metallo-organic precursors; Mixed oxides; Antiferromagnets; Weak ferromagnetism

1. Introduction

The study of perovskite-related mixed oxides was prompted by the discovery of high-temperature superconductors and magnetoresistive oxides [1,2], with presence of mixed valence transition metals. In non-stoichiometric ABO_{3-x} oxides with perovskite-type structure, when a transition ion such as manganese is incorporated into a crystal lattice along with cations such as calcium, the higher-valence states are easily stabilized giving rise to the $Ca(Mn^{3+}/Mn^{4+})O_{3-x}$ mixed oxides which exhibit interesting electric and magnetic properties [3–5]. The $CaMnO_{3-x}$ ($0 \leqslant x \leqslant 0.5$) phases exhibit structures related to the perovskite with oxygen vacancies which affect, in a significant way, the magnetic and electronic properties [6]. The stoichiometric oxide, $CaMnO_3$, has an orthorhombic perovskite structure ($\sqrt{2}a_c, 2a_c, \sqrt{2}a_c$) and is a G-type antiferromagnetic insulator, with a Néel temperature of 120 K [4]. This oxide also exhibits weak ferromagnetism below Néel temperature, attributed to a canted spin structure [3]. With decreasing the oxygen content, the $CaMnO_{3-x}$ phases show stronger ferromagnetic interactions with a slight increase in the $T_{Néel}$ [6] and an increase in the conductivity, becoming *n*-type semiconductors [5]. Both effects are explained by the incorporation of Mn^{3+} cations when the oxides are reduced, which induces Mn^{3+}–O–Mn^{4+} ferromagnetic double-exchange interactions [7] and conduction by electron hopping [5]. Furthermore, some authors have recently related both effects and have found magnetoresistive properties in these phases [8]. More recently, important works have been published concerning the effect of doping the manganese sites by pentavalent or hexavalent cations such as Re, Ru, Nb, Ta, W or Mo, in order to introduce Mn^{3+} in a low concentration [9–12]. The resulting properties observed in these $CaMn_{1-x}M_xO_{3-\delta}$ phases are similar to those obtained in the non-stoichiometric $CaMnO_{3-x}$ phases, attributable to the presence of some Mn^{3+} cations.

*Corresponding author. Fax: +34-94-4648-500.
E-mail address: qiproapt@lg.ehu.es (T. Rojo).

0022-4596/$ - see front matter © 2004 Elsevier Inc. All rights reserved.
doi:10.1016/j.jssc.2004.06.052

The synthesis of these $CaMnO_{3-x}$ oxides described in the literature was usually performed by conventional solid-state reactions involving high temperatures and long reaction times, obtaining samples with large particle size. In this way, the $CaMnO_{3-x}$ oxides have been synthesized at temperatures above 1100 °C, and at lower temperatures, near 900 °C, by using carbonate precursors [13], or using the Pechini citrate gel process [14,15].

The thermal decomposition of metallo-organic precursors allowed us to prepare metastable or stable phases at lower temperatures containing smaller grain sizes than those obtained from the ceramic method [16,17]. By this method, the diffusion distances are remarkably reduced and, as a consequence, the reaction times and temperatures. The obtained product presents more quality, being highly homogeneous and the grain size considerably smaller [18]. Although different ligands can be used in the synthesis of these compounds, the carboxylate ligands have often been used to complex the transition metal ions [19–21]. In this way, malonate is a good bridging ligand extensively used due to the facility to form polynuclear complexes [22,23].

In this paper, we present the synthesis and characterization of the $CaMnO_{3-x}$ oxides obtained by thermal treatments from the previously characterized $[CaMn(C_3H_2O_4)_2(H_2O)_4]$ precursor [24], together with the ceramic method, with the aim of studying the influence of the synthesis method on the properties. The samples have been identified by X-ray powder diffraction and their morphological and magnetic properties have been investigated.

2. Experimental

2.1. Synthesis

The oxides were synthesized by thermal decomposition of a metallo-organic precursor and ceramic method. The metallo-organic precursor $[CaMn(C_3H_2O_4)_2(H_2O)_4]$ was obtained by mixing stoichiometric quantities of calcium chloride and manganese (II) nitrate, with malonic acid neutralized with sodium carbonate, as previously described [24]. Calcium chloride, manganese (II) nitrate, and malonic acid were purchased from Aldrich Co. and sodium carbonate from Merck. Then, the malonate precursor was fired in a tubular furnace at 400 °C for 12 h to remove the organic part, followed by treatments at 800 °C in air and in oxygen. The conventional ceramic process was also used. Stoichiometric quantities of calcium and manganese carbonates were mixed in an agate mortar and heated at 1350 °C during 50 h in air to obtain the pure phase $CaMnO_{3-x}$. Manganese (II) carbonate was purchased from Aldrich Co. and calcium carbonate from Merck. All the reactants were used without further purification.

2.2. Physical measurements

Analytical measurements were carried out in an ARL 3410 + ICP with Minitorch equipment. Thermogravimetric measurements were performed in a TA instruments-STD 2960 thermobalance. Approximately 15–20 mg of sample were placed on an alumina crucible and heated to 900 °C at 5 °C/min, in synthetic air and nitrogen atmosphere in the case of the precursors and at 5 °C/min in flowing 5% H_2/Ar for the oxides. Scanning electron microscopic (SEM) and transmission electron microscopic (TEM) photographs were taken in order to get some indication of the compactness of the oxide, using a JEOL JSM-6400 and a Philips CM200, respectively. The powder X-ray diffraction (XRD) patterns were taken using a Philips X-PERT diffractometer with Cu$k\alpha_1$ radiation. Data were collected by scanning in the range $10° < 2\theta < 100°$ with increments of 0.03° (2θ) during 15–16 s. ESR spectra were recorded on a Bruker ESP 300 spectrometer, equipped with a standard Oxford low-temperature device operating at X and Q bands. The magnetic field was measured with a Bruker BNM 200 gaussmeter, and the frequency was determined with an HP5352B-microwave frequency counter. Magnetic and resistance measurements were performed in the temperature range 4.2–300 K using a QUANTUM DESIGN MPMS-7 SQUID magnetometer. The magnetic measurements were performed at magnetic fields up to 7 T.

3. Results and discussion

3.1. Thermal analysis of the precursors

Thermal data of the $[CaMn(C_3H_2O_4)_2(H_2O)_4]$ compound were obtained from their TG curves in air and nitrogen atmospheres that are shown in Fig. 1a. Decomposition occurs following three consecutive processes, dehydration, ligand pyrolysis and inorganic residue formation.

The first process takes place in the 145–245 °C temperature range for both atmospheres and corresponds to the loss of the four water molecules present in the complex. This process occurs in only one step, suggesting that all the water molecules are similar as was deduced from the crystallographic data of the $[CaMn(C_3H_2O_4)_2(H_2O)_4]$ compound [24]. After that, the decarboxylation of the ligand comes as a sharp mass loss in the 350–450 °C temperature range. This process takes places more progressively in N_2 atmosphere. The weight loss agrees with the decarboxylation of the malonate ligand to yield $CaCO_3$ and the corresponding

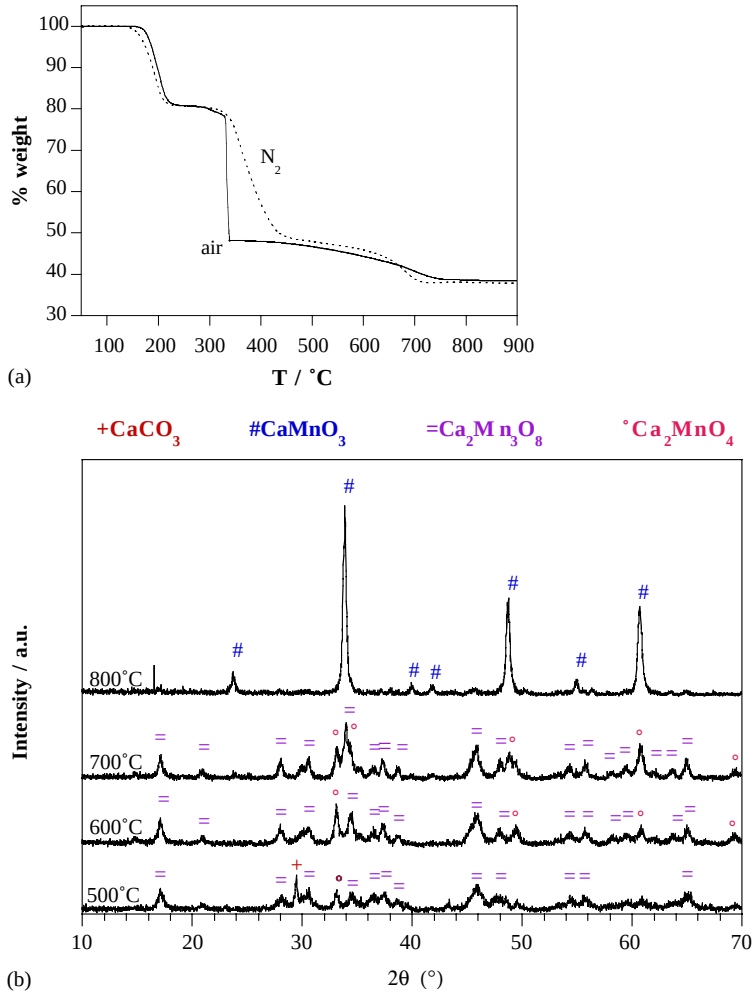

Fig. 1. (a) TG curves in air and nitrogen, and (b) XRD pattern of the phases obtained at different temperatures from the $[CaM(C_3H_2O_4)_2(H_2O)_4]$ precursor.

transition metal oxides. These oxides mainly depend on the applied atmosphere. In this way, oxides with higher MnO_2 and lower MnO oxidation states were formed in air and nitrogen atmospheres, respectively.

In the 600–800 °C range, the evolution of the inorganic residue shows a gradual mass loss, due to the decomposition of the carbonate and the formation of the mixed oxides, and finishes in an interval of stability. The resulting residues were analyzed by XRD, indicating the presence of the $CaMnO_{3-x}$ [25] phase in both air and nitrogen atmospheres. That is, the last weight-constant *plateau* corresponds to the formation of a stable $CaMnO_{3-x}$ oxide.

3.2. Formation of the mixed oxide

Following this study and in order to obtain pure phases of mixed oxides, thermal treatments in tubular furnaces were carried out. After firing the CaMn malonate precursor at 400 °C, treatments at higher temperatures during 2 h were performed. The resulting products in each stage were characterizated by X-ray powder diffraction (see Fig. 1b). The thermal decomposition of $[CaMn(C_3H_2O_4)_2(H_2O)_4]$ at 600 and 700 °C gave rise to the formation of mixed oxides such as $Ca_2Mn_3O_8$ [26] and Ca_2MnO_4 [27]. Finally, the $CaMnO_3$ [25] oxide was obtained as pure phase at 800 °C.

Taking into account these results, two syntheses in different atmospheres, air and oxygen, have been performed at 800 °C for 15 h, with the aim of varying the oxygen content in $CaMnO_{3-x}$. This phase was also obtained by the ceramic method for comparison, at higher temperatures (1350 °C) during 2 days.

The oxygen stoichiometry of the three samples was determined by thermogravimetric analysis, the oxides were heated to 900°C in flowing 5% H_2/Ar [28]. The samples were reduced to $CaMnO_2$ and the weight losses observed agreed with the $CaMnO_3$ stoichiometric phase for the samples obtained from the precursor in air and in oxygen, and with $CaMnO_{2.98}$ ($CaMn^{4+}_{0.96}Mn^{3+}_{0.04}O_{2.98}$) for

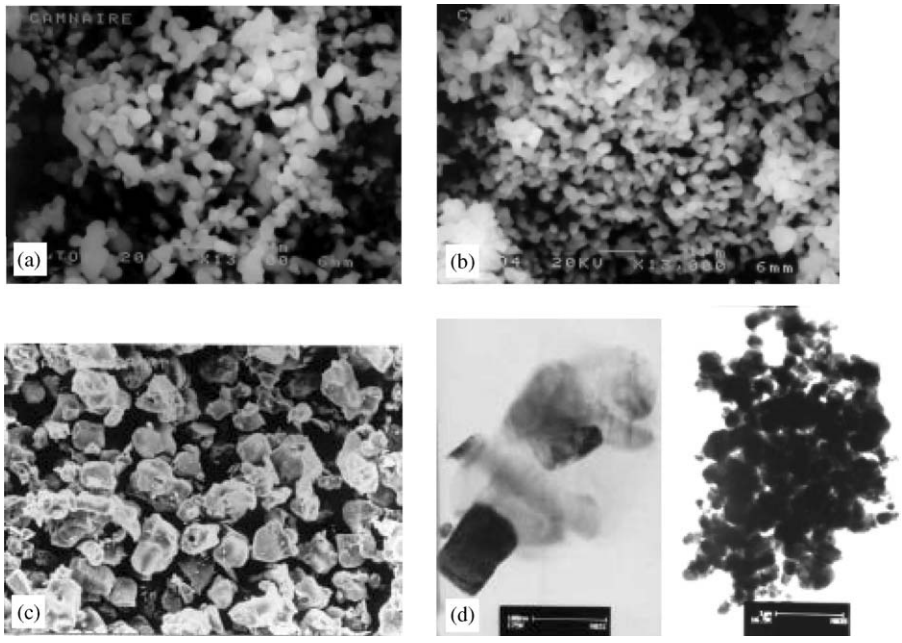

Fig. 2. SEM photographs of $CaMnO_{3-x}$ oxides obtained (a) in air ($\times 13000$), (b) in oxygen ($\times 13000$), and (c) in air by the ceramic method ($\times 1000$). (d) TEM photographs of $CaMnO_3$ oxide obtained in oxygen.

that prepared by the ceramic synthesis. In these phases, the oxygen stoichiometry is directly affected by the synthesis method, especially by the temperature of synthesis. Therefore, the advantage of the precursor route is that it allows both lower temperatures and times of reaction, giving rise to more oxidized oxides, in good agreement with other studies [14]. In this case, an oxidant atmosphere has not been necessary in order to obtain the more oxidized $CaMnO_3$ stoichiometric phase.

The morphology of the samples was analyzed by SEM and TEM (Fig. 2). The polycrystalline powders of the $CaMnO_3$ oxides obtained from the metallo-organic precursors at 800°C are formed by small, 100–200 nm, and highly homogeneous particles, which tend to form conglomerates. This morphology of small homogeneous particles, near nanoscale, is very reactive and sensitive for compaction and it is also a consequence of the soft synthesis routes, low temperatures and short reaction times. The grain size of the sample obtained by the ceramic method at 1350° C is 100 times higher, 10–30 μm, being quite homogeneous. In general, the more the temperature increases the higher the size of the particles.

The XRD patterns of the three phases were analyzed by the FULLPROF program [29] on the basis of the orthorhombic unit cell, *Pnma,* and using the initial atomic positions proposed by Taguchi [30] (Fig. 3). The refined parameters and some bonds and angles are summarized in Tables 1 and 2. Unfortunately, the accuracy of the data is not very good. The deviations of the bond distances and angles are not small and the R_{Bragg} and R_f reliability factors are larger for the sample obtained by the ceramic route in relation to the compounds obtained by the precursor route, so these results must be taken cautiously. As can be seen, the six Mn–O distances are quite similar in the three phases. However, in the phase obtained by the ceramic synthesis the Mn–O–Mn angles are more different from each other. Therefore, it seems that the more distorted structure is exhibited by the $CaMnO_{2.98}$ phase obtained by the ceramic synthesis, which is consistent with the presence of some oxygen vacancies ($\delta = 0.02$) by the reduction of Mn^{4+} to Mn^{3+}. The small increment of the cell volume would be also in agreement with the increase of Mn^{3+} content and the increased Shannon effective ionic radii [31] of Mn^{3+} (0.645 Å) relative to that of Mn^{4+} (0.53 Å), and the degree of distortion with the deviation of the tolerance factor $t = (r_{Ca} + r_O)/\sqrt{2}(r_{Mn} + r_O)$.

3.3. Spectroscopic and magnetic properties of the $CaMnO_{3-x}$ oxides

The ESR spectra were recorded at X band and at different temperatures between 4.2 and 290 K for the three samples. Very similar results were observed in the three cases. In Fig. 4 it is shown that the thermal evolution of the ESR normalized signals until 100 K of the sample $CaMnO_3$ synthesized in air from the precursor, together with the evolution of the intensity and linewidth. An isotropic signal centered at Landé factor $g \approx 2$ with a peak-to-peak linewidth ΔH_{pp} value

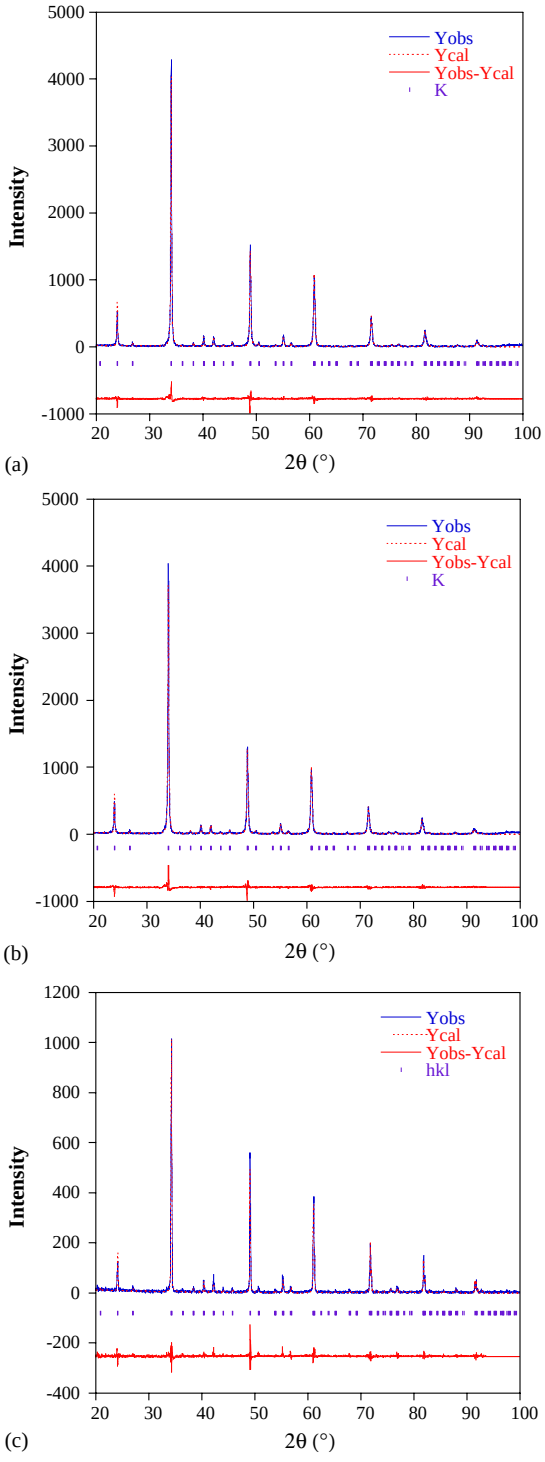

Fig. 3. X-ray powder diffraction data and Rietveld refinement profile for $CaMnO_{3-x}$ oxide obtained in (a) air, and (b) oxygen from the metallo-organic precursor. (c) The diffractogram of the compound obtained by the ceramic method.

of 1240 G appears at room temperature. The g value remains unchanged with decreasing temperature, whereas the linewidth gradually increases, except in the 160–130 K temperature range, where it unexpectedly

Table 1
Refined cell parameters (Å) and reliability factors

	$CaMnO_3$ in air	$CaMnO_3$ in O_2	$CaMnO_{2.98}$ ceramic
a	5.2827(5)	5.2812(8)	5.2715(1)
b	7.4576(8)	7.457(1)	7.4619(2)
c	5.2735(5)	5.2753(8)	5.2859(1)
V	207.76(4)	207.75(5)	207.92(1)
χ^2 (Å^2)	1.78	1.82	1.51
R_{Bragg} (Å^2)	4.04	4.04	8.47
R_f (Å^2)	3.86	4.32	8.20

decreases. The increase of the linewidth is related to the presence of spin couplings, and considering the slow increase, a gradual coupling (or short-range coupling) may be proposed from room temperature to 100 K. The intensity of the signal slightly increases when lowering the temperature up to 130 K; at this point, it abruptly falls, making ESR silent below 100 K. The intensity is related to the quantity of parallel or antiparallel oriented magnetic moments. Therefore, the fall of the intensity below 130 K can be explained as due to the presence of antiferromagnetic couplings below this temperature as main interactions. Consequently, the antiparallel ordering of the spins should originate the disappearance of the signal at low temperatures.

Magnetic measurements of the $CaMnO_{3-x}$ samples were carried out in the 4.2–300 K temperature range. The field cooled FC and zero field cooled ZFC magnetization curves are shown in Fig. 5. It is worth mentioning the sudden increase observed at 120 K in all ZFC curves. This increase and the differences observed between the two FC and ZFC curves suggest the existence of a magnetic transition at this temperature. At room temperature, the values of the calculated magnetic moments ($\mu_{eff} = \sqrt{8\chi mT}$), 2.66–2.75 μ_B, are slightly lower than that expected for an Mn^{4+} system. This fact, together with the slow initial decrease of the magnetic moment, can be indicative of the existence of short-range antiferromagnetic interactions. Moreover, the inverse of the susceptibility does not fit the Curie–Weiss behavior, confirming the presence of magnetic interactions in all the range of temperatures studied, in good agreement with the ESR data. After that, the rapid increase of the magnetic moments at 120 K, followed by the hysteresis between the ZFC and FC curves, indicates the presence of a ferromagnetic component simultaneous to the establishment of a whole antiferromagnetic ordering. The Néel temperature, near 120 K, is the same for the three samples in good agreement with the data reported in the literature [3,4,6]. The M/H curves measured at different fields show that the magnetization is highly dependent on the applied field, this dependency being clearer in the case of

Table 2
Refined atomic positional parameters and selected distances Mn–O (Å) and Mn–O–Mn angles (deg)

Atom	$CaMnO_3$ in air			$CaMnO_3$ in O_2			$CaMnO_{2.98}$ ceramic		
	x	y	z	x	y	z	x	y	z
Ca	0.0290(6)	$\frac{1}{4}$	−0.009(2)	0.0288(6)	$\frac{1}{4}$	−0.008(2)	0.0248(1)	$\frac{1}{4}$	−0.001(2)
Mn	0	0	$\frac{1}{2}$	0	0	$\frac{1}{2}$	0	0	$\frac{1}{2}$
O(1)	0.488(2)	$\frac{1}{4}$	0.064(3)	0.489(2)	$\frac{1}{4}$	0.067(3)	0.477(3)	$\frac{1}{4}$	0.038(5)
O(2)	0.286(3)	0.030(2)	0.709(2)	0.285(3)	0.033(2)	0.711(3)	0.291(3)	0.047(2)	0.712(3)
Mn–O(1) × 2	1.896(3)			1.898(3)			1.880(3)		
Mn–O(2) × 2	1.88(1)			1.89(1)			1.94(2)		
Mn–O(2) × 2	1.92(1)			1.91(1)			1.91(2)		
Mn–O(1)–Mn	159.0(1)			158.3(1)			165.6(1)		
Mn–O(2)–Mn	157.9(6)			157.4(6)			152.4(7)		

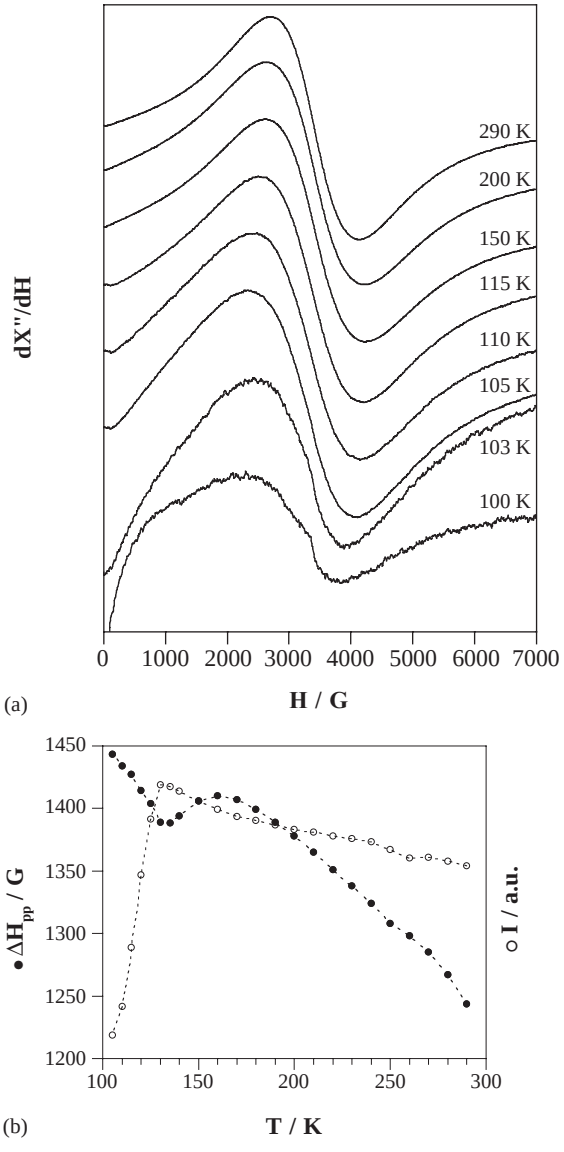

Fig. 4. (a) X band ESR spectra at different temperatures, and (b) thermal evolution of the peak-to-peak linewidth (ΔH_{pp}) (●) and the intensity of the signals (○) for the $CaMnO_3$ oxide obtained in air. The other samples showed very similar curves.

the oxide obtained from the ceramic synthesis. At stronger fields the ferromagnetic component diminishes, so this component comes into being as a result of the antiferromagnetic ordering. Anyway, the values reached at 4.2 K are very low, suggesting a weak nature for the ferromagnetic interaction. Finally, the local maximum observed at low temperature in the FC curves of the sample prepared by the ceramic route suggests a possible frustration effect induced by a competition from different magnetic interactions. This fact could be consistent with the presence of some Mn^{3+}–O–Mn^{4+} ferromagnetic clusters as some authors had previously described [9,16].

In order to study this ferromagnetic component, magnetization vs. magnetic field measurements were carried out at different temperatures. The magnetization hysteresis loops measured at 5 K are represented in Fig. 6. The dependence with the magnetic field is linear at room temperature, corroborating the antiferromagnetic character of the samples at this temperature. At 120 K, a small hysteresis loop appears which remains with decreasing temperature. The coercive field and the saturation magnetization values measured at 120 K for the oxide obtained from the precursor, 1500 Oe and 0.008 (in Nβ units), increase with decreasing temperature, until $H_c = 8500$ Oe and $M_s = 0.025$ (in Nβ units) values at 5 K. In the case of the ceramic case, the hysteresis loop obtained at 5 K is quite surprising, characteristic of materials with soft magnetic properties. The coercive field is very small, near 700 Oe, and the saturation magnetization value is higher, 0.03 (in Nβ units). This narrow cycle is in accordance with the absence of the antiferromagnetic peak in the ZFC data at T_N and indicates that the anisotropy energy holding the spins along the preferred direction must have a low barrier for spin canting away from this direction in this phase. Anyway, taking into account the values of the saturation magnetization as well as the susceptibility data, the magnitude of the parallel alignment will be very small.

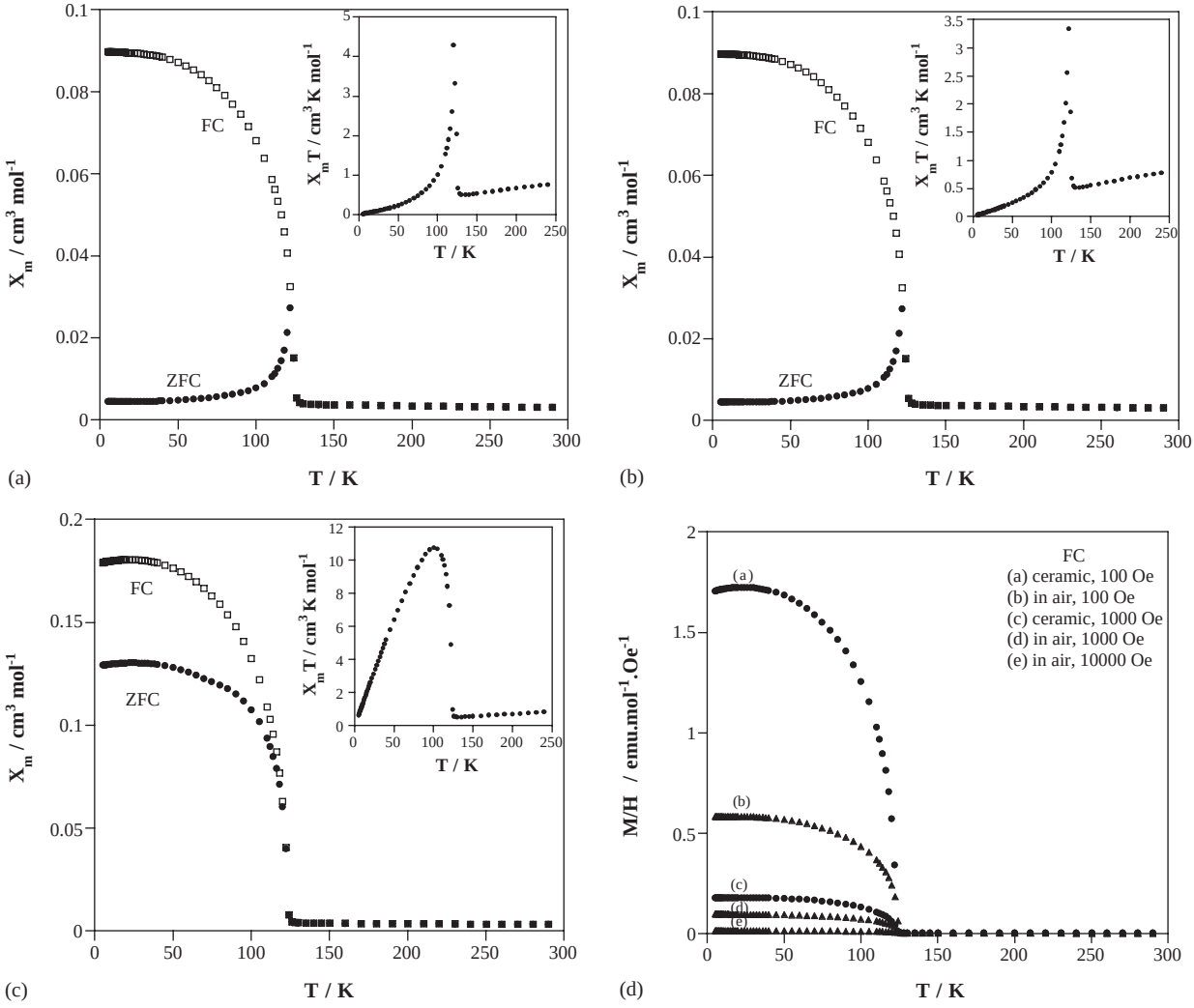

Fig. 5. FC and ZFC curves measured under a magnetic field of 1000 G for $CaMnO_{3-x}$ oxide obtained (a) in air, (b) in oxygen, and (c) in air by the ceramic method. Thermal evolution of the $\chi_m T$ data is represented in the insets. (d) M/H vs. T curves measured at different fields.

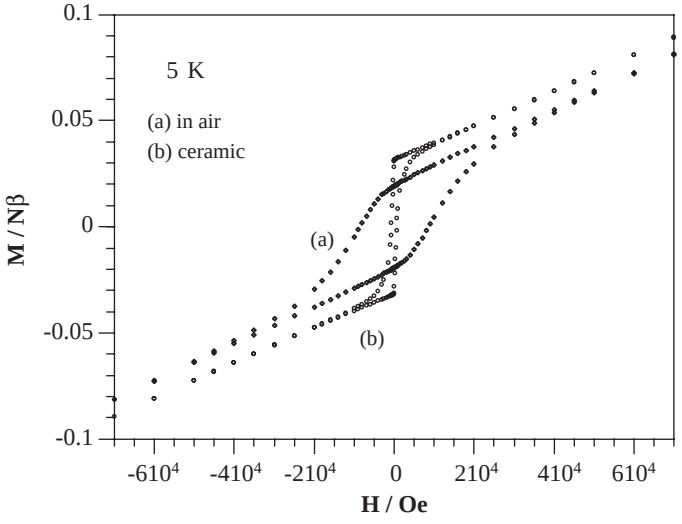

Fig. 6. Magnetization vs. applied magnetic field at 5 K for the $CaMnO_{3-x}$ phases.

The existence of this ferromagnetic component can be mainly interpreted as due to the presence of a field-induced spin canting originated in the antiferromagnetic phase by a misalignment of the spins, as a consequence of the O–Mn–O (below 160°) distorted angle [3], more distorted in the $CaMnO_{2.98}$ case. Furthermore, in this phase, some localized Mn^{3+}–O–Mn^{4+} double-exchange ferromagnetic interactions could also contribute to the ferromagnetic component, similar to those found in magnetorresistant perovskites [32].

Finally, the method of preparation used to obtain these materials and the final morphology of the products have been found to be important factors in order to explain the properties. In this sense, homogeneous products have been obtained in the three cases, not only morphologically but also compositionally homogeneous, as the immediate responses in the magnetization curves indicate. On the other hand, considering both the intergrain and intragrain transmission of the magnetic properties, the higher grain size in the ceramic sample leads to higher magnetic moments inside each grain and to higher net magnetic moments; therefore, it seems that the alignment of the spins takes place more easily inside each small particle than through grain boundary transmission. Moreover, the soft magnetic properties found in this sample can also be related to the grain size. The higher the grain, the better the co-operation between the different magnetic dominions and the quicker the response of the sample to a change in the applied magnetic field.

4. Conclusion

The method of synthesis plays an important role in the oxygen stoichiometry of the $CaMnO_{3-x}$ phases, especially the temperature of synthesis. In this sense, the precursor route has been shown as convenient route to obtain the most oxidized oxide, the stoichiometric $CaMnO_3$, as a very fine and homogeneous powder, at low temperatures and short reaction times. The ceramic process gives rise to the attainment of the non-stoichiometric $CaMnO_{2.98}$ oxide with more distorted structure and a grain size 100 times higher. In both cases, the products obtained are highly homogeneous.

At the same time, the oxygen stoichiometry and morphology of the different samples affect the magnetic properties. Although the samples obtained from the precursor and the ceramic method show similar magnetic properties, low-dimensional antiferromagnetic interactions at high temperatures followed by a three-dimensional antiferromagnetic ordering with a $T_{Néel}$ near 120 K and weak ferromagnetism due to spin canting at lower temperatures, this latter component is stronger in the ceramic case. This variation is mainly related to the more distorted structure found in the non-stoichiometric oxide and secondly, to the presence of some Mn^{3+}–O–Mn^{4+} ferromagnetic clusters.

Acknowledgments

This work has been carried out with the financial support of the Ministerio de Ciencia y Tecnología MCyT (MAT2001-0064)) and the Universidad del País Vasco/Euskal Herriko Unibertsitatea (9/UPV00169.310-14199/2001). The authors would also like to thank Prof. M.L. Nó for providing user time of the electronic microscopes.

References

[1] S. Jin, T.H. Tiefel, M. McCormack, R.A. Fastnacht, R. Ramesh, L.H. Chen, Science 264 (1994) 413.
[2] R. von Helmolt, J. Wecker, B. Holzapfel, L. Schultz, K. Samwer, Phys. Rev. Lett. 71 (1993) 2331.
[3] J.B. MacChesney, H.J. Williams, J.F. Porter, R.C. Sherwood, Phys. Rev. 164 (2) (1967) 545.
[4] E.O. Wollan, W.C. Koehler, Phys. Rev. 100 (2) (1955) 545.
[5] H. Taguchi, Phys. Stat. Sol. (a) 88 (1985) K79.
[6] J.B. Goodenough, Phys. Rev. 100 (2) (1955) 564.
[7] J. Briático, B. Alascio, R. Allub, A. Butera, A. Caneiro, M.T. Causa, M. Tovar, Phys. Rev. B 53 (21) (1996) 14020.
[8] Z. Zeng, M. Greenblatt, M. Croft, Phys. Rev. B 59 (13) (1999) 8784.
[9] B. Raveau, Y.M. Zhao, C. Martin, M. Hervieu, A. Maignan, J. Solid State Chem. 149 (2000) 203.
[10] B. Raveau, A. Maignan, C. Martin, M. Hervieu, Mater. Res. Bull. 35 (2000) 1579.
[11] A. Maignan, M. Martin, M. Hervieu, B. Raveau, Solid State Commun. 117 (2001) 377.
[12] A. Maignan, M. Martin, C. Autret, M. Hervieu, B. Raveau, J. Hejtmanek, J. Mater. Chem. 12 (2002) 1806.
[13] H.S. Horowitz, J.M. Longo, Mater. Res. Bull. 13 (1978) 1359.
[14] M.E. Melo Jorge, A. Correia dos Santos, M.R. Nunes, Int. J. Inorg. Mater. 3 (2001) 915.
[15] I.D. Fawcett, J.E. Sunstrom IV, M. Greenblatt, Chem. Mater. 10 (1998) 3643.
[16] C.N.R. Rao, Chemical Approaches to the Synthesis of Inorganic Materials, Wiley, New York, 1994.
[17] K. Vidyasagar, J. Gopalakrishnan, C.N.R. Rao, Inorg. Chem. 23 (1984) 1206.
[18] F.F. Lange, in: Chemical Processing of Advanced Materials, Wiley, New York, 1992.
[19] M. Insausti, R. Cortés, M.I. Arriortua, T. Rojo, E.H. Bocanegra, Solid State Ionics 63–65 (1993) 351.
[20] M. Insausti, J.L. Pizarro, L. Lezama, R. Cortés, E.H. Bocanegra, M.I. Arriortua, T. Rojo, Chem. Mater. 6 (5) (1994) 707.
[21] J. García-Jaca, J.I.R. Larramendi, M. Insausti, M.I. Arriortua, T. Rojo, J. Mater. Chem. 5 (11) (1995) 1995.
[22] I. Gil de Muro, F.A. Mautner, M. Insausti, L. Lezama, M.I. Arriortua, T. Rojo, Inorg. Chem. 37 (1998) 3243.
[23] I. Gil de Muro, M. Insausti, L. Lezama, J.L. Pizarro, M.I. Arriortua, T. Rojo, Eur. J. Inorg. Chem. (1999) 935.
[24] I. Gil de Muro, M. Insausti, L. Lezama, M.K. Urtiaga, M.I. Arriortua, T. Rojo, J. Chem. Soc. Dalton Trans. 19 (2000) 3360.
[25] Powder Diffraction File, Card No 3–830, JCPDS, Swarthmore, PA, 1995.

[26] Powder Diffraction File, Card No 34–469, JCPDS, Swarthmore, PA, 1995.
[27] Powder Diffraction File, Card No 24–1194, JCPDS, Swarthmore, PA, 1995.
[28] K.R. Poeppelmeier, M.E. Leonowicz, J.M. Longo, J. Solid State Chem. 44 (1982) 89.
[29] J. Rodriguez-Carvajal, FULLPROF. Program Rietveld Pattern Matching, Analysis of Powder Patterns, Grenoble, IL, Nonpublished, 1994.
[30] H. Taguchi, J. Solid State Chem. 124 (1996) 360.
[31] R.D. Shanonn, Acta Crystallogr. A 32 (1976) 751.
[32] J.M.D. Coey, M. Viret, S. von Molnár, Adv. Phys. 48 (2) (1999) 167.